ChemPubSoc Europe

DOI: 10.1002/ejic.201800663

EurJIC European Journal of Inorganic Chemistry

Full Paper

Aqueous Glucose Reforming

Photocatalytic Solar Light H_2 Production by Aqueous Glucose Reforming

Marianna Bellardita,*[a] Elisa Isabel García-López,[a] Giuseppe Marcì,[a] Giorgio Nasillo,[b] and Leonardo Palmisano*[a]

Abstract: A series of tungsten and nitrogen doped Pt-TiO_2 samples were prepared with the aim to extend the TiO_2 absorption to the visible light region and to enhance the separation efficiency of the photogenerated electron/hole pairs. The physicochemical features of the powders were characterized by X-ray diffraction (XRD), UV/Vis reflectance spectra, specific surface area (SSA) determinations, and transmission electron microscopy (TEM) analyses. The influence of the presence of different doping agents was evaluated, under anaerobic conditions, in the aqueous photo-reforming of glucose to form H_2 at ambient pressure and temperature under a halogen lamp or natural solar light irradiation. Arabinose, erythrose, and formic acid were the main glucose partial oxidation products observed in the liquid phase, whilst H_2 and CO_2 were measured in the gaseous phase. The highest H_2 production was observed in the presence of the Pt-TiO_2-W0.25 sample.

1. Introduction

In the last decades, there has been a growing interest in renewable energy sources, due to both the almost exhaustion of the fossil fuels currently used, and the growth of environmental pollution with damaging effects for the ecosystem and health of people. The use of renewable sources can efficiently help to solve these issues and, among them, hydrogen is a clean energy carrier, because its combustion with oxygen produces only water.[1–3]

Nowadays, the dominant industrial processes for hydrogen production are steam reforming from hydrocarbons,[1] biomass conversion processes (such as direct combustion, gasification, pyrolysis)[4–6] and water splitting by means of different technologies: electrolysis, radiolysis, thermolysis, photobiology and photocatalysis.[7,8] Most of these methods are not economically sustainable as they require large equipment, high temperature and pressure, and significant energy consumption.[9]

To ensure that this new energy carrier is effectively "green", hydrogen production has to be as clean as possible. In this scenario heterogeneous photocatalysis, under ambient conditions and in the presence of green solvents and sunlight irradiation, represents one of the cleanest way to directly split water into hydrogen and oxygen.[10–12] Unfortunately, the direct water splitting is a very hard and disadvantageous process by a thermodynamic and kinetic point of view. Biomass conversion is less energy demanding than water splitting. The use of glucose, glycerol, lignin, etc., as sacrificial agents, can reduce the electron/hole recombination rate and favour selectively the synthesis of high value-added products.[6,13–22] There are still only a relative small number of materials that can efficiently photoreform biomass, and works dedicated to improving the efficiency of photocatalysts, especially under natural solar light irradiation, are useful. TiO_2 is the most employed photocatalyst for this process because of its low cost, chemical and photochemical stabilities, and ease of preparation.[16,23]

TiO_2 photoactivation presents some weaknesses due to its high electron/hole recombination rate and the need of UV light.[24] Many approaches have been explored to improve the TiO_2 efficiency and to better exploit the solar radiation, as doping with metal[25–27] and non-metal species,[28–30] co-doping,[31–33] surface modification by organic species sensitization,[34,35] coupling of different semiconductors.[36–39]

Among the nonmetallic elements, since the work of Asahi et al.,[40] a great attention has been addressed to N doped TiO_2 because it is reported that the band gap of TiO_2 becomes smaller, due to formation of a mid-gap energy state above the valence band[41–43] and presence of oxygen vacancies generating color centers.[44] N-TiO_2 samples have been employed also for glucose photo-reforming.[45–46] Ilie et al.[45] compared the photoactivity of a series of Au-TiO_2 samples dispersed on SiO_2 and doped with metal (Mn, Cr, V) or non-metal (N or S) species towards the H_2 production from aqueous sugar solution. The best results were obtained in the presence of non-metals and were attributed to a lower tendency to form recombination centers with respect to samples doped with metals.

As far as the metallic species are concerned, tungsten has attracted the attention of many researchers because the pres-

[a] "Schiavello-Grillone" Photocatalysis Group, Dipartimento di Energia, Ingegneria dell'informazione, e modelli Matematici (DEIM), Università degli Studi di Palermo,
Viale delle Scienze Ed. 6, 90128, Palermo, Italy
E-mails: marianna.bellardita@unipa.it, leonardo.palmisano@unipa.it
http://www.unipa.it/photocatalysis

[b] Laboratorio di Microscopia Elettronica a Trasmissione-Advanced Technologies Network Center (ATeN), University of Palermo,
Viale delle Scienze Ed. 17, 90128, Palermo, Italy

ORCID(s) from the author(s) for this article is/are available on the WWW under https://doi.org/10.1002/ejic.201800663.

ence of WO_3 in the TiO_2 lattice can enhance the separation efficiency of the photogenerated charges, while the presence of cations (W^{6+} and/or W^{4+}) substituting Ti^{4+} ions, can modify the TiO_2 electronic structure.[47,48] Due to the different behaviour of metals and non-metals, co-doping was used as a strategy to enhance the photocatalytic activity of TiO_2.[33,49–52] It is reported that anions and cations generate shallow localized levels near the valence and conduction band edges, allowing the band gap decrease and the shift of the two bands towards less positive and less negative values, respectively.[53] Various N, W co-doped TiO_2 systems have been prepared and tested under solar light irradiation for oxidation reactions.[54–57] In those cases, isolated N *2p* states are located above the valence band edge whilst W *5d* states below the conduction band edge.

The obtainment of high value-added chemicals from biomass derived compounds has been the subject of intense research in recent years.[58–59] In this context the use of glucose appears interesting because it is an abundant and cheap monosaccharide.

The aim of the work reported in this paper was to synthesize Pt-TiO_2-rutile based materials doped with N or W species which were used under ultraviolet (UV), halogen lamp (HL) or natural solar light (SOL) irradiations to obtain H_2 by photo-reforming of a glucose aqueous solution. Rutile TiO_2 polymorph was chosen because it has been reported to show a photocatalytic H_2 production efficiency higher than that of the anatase phase, under similar experimental conditions.[22]

2. Results and Discussion

2.1 Characterization of the Photocatalysts

The XRD patterns of the pristine and doped samples are shown in Figure 1. The bare TiO_2 consisted of pure rutile; the presence of nitrogen did not alter the phase composition (Figure 1A), whilst the appearance of anatase was observed in the presence of tungsten, and it increased with the amount of the dopant (Figure 1B), according to what previously observed.[60] Broad peaks were obtained, suggesting a poor crystallinity of the samples due to the low preparation temperature. The absence of peaks related to N and W species can be ascribed to the low amount of dopants and to a high degree of dispersion of the loaded species on the TiO_2 surface. The crystallites size ranged between 5.6 and 12.5 nm (Table 1) and the highest values were measured for the samples containing the highest percentages of dopant species. The slight broadening of the peaks after doping may be due to the formation of structural defects in the presence of foreign ions.

Table 1. Phase composition, crystallite size (Φ), band-gap (E_g), specific surface areas (SSA) of the prepared samples (in brackets the mid-gap values are reported).

Sample	Phase	Φ [nm]	E_g [eV]	SSA [$m^2\ g^{-1}$]
TiO_2	R	5.6	2.98	21
Pt-TiO_2	R	7.7	2.90 (2.45)	7
Pt-TiO_2-N0.5	R	7.9	2.86 (2.47)	1
Pt-TiO_2-N1	R	12.5	2.74 (2.41)	≈ 1
Pt-TiO_2-N2	R	12.1	2.72 (2.42)	≈ 1
Pt-TiO_2-W0.25	R	8.8	3.26 (2.95)	66
Pt-TiO_2-W0.5	R+A	7.7	3.16 (2.96)	64
Pt-TiO_2-W1	R+A	12.4	2.92 (2.57)	18
Pt-TiO_2-W2	A+R	10.3	2.86 (2.49)	28
Pt-TiO_2-N0.5W0.5	R	7.5	2.88 (2.48)	3.4

The bare TiO_2 exhibited a specific surface area (SSA) of 21 $m^2\ g^{-1}$, that decreased in the presence of Pt and nitrogen, whilst an increase was observed when W was loaded. The samples containing N showed very low values of SSA (about 1 $m^2\ g^{-1}$), and when tungsten was present, the increase was

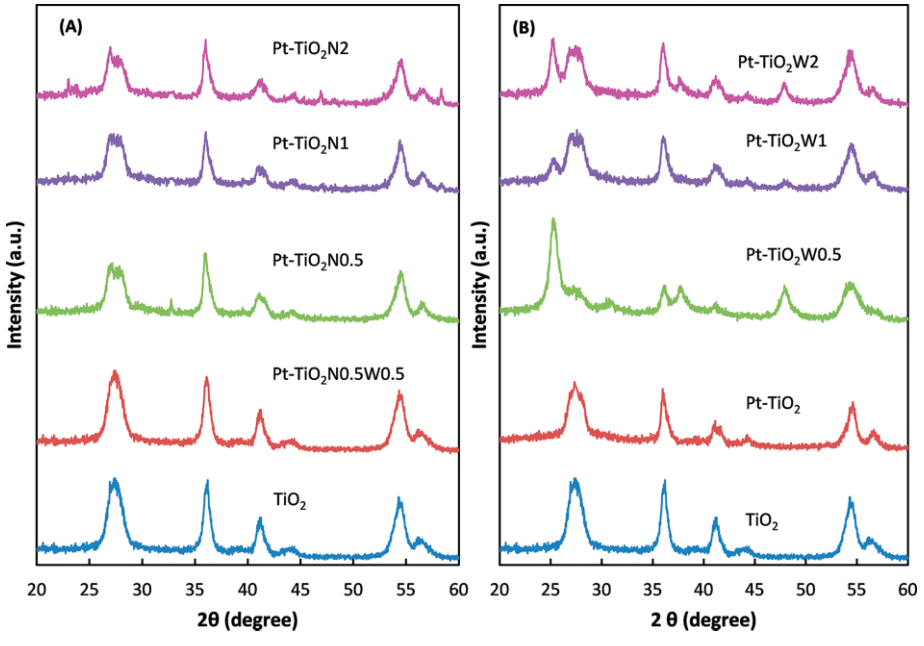

Figure 1. XRD patterns of N-doped (A) and W-doped (B) TiO_2 samples. A = Anatase, R = Rutile.

the highest in the presence of the lowest amounts of metal (0.25 and 0.5 weight %) whilst only small variations occurred with the highest quantities. The pore volume was 0.018 $cm^3 g^{-1}$ for pristine TiO_2, decreased by adding Pt (0.005 $cm^3 g^{-1}$) and further with nitrogen down to 0.003 $cm^3 g^{-1}$ whilst an increase occurred in the presence of tungsten, reaching the value of 0.03 $cm^3 g^{-1}$. The increase of the pore volume for the W-doped samples with respect to the N-doped ones (0.03 vs. 0.003 $cm^3 g^{-1}$) may partly justify the higher surface areas of the first samples, although the crystallites size for all of the doped samples is not dramatically different. The surface area and pore volume decrease observed after addition of Pt can be due to the pore blockage by the metal. Their variation in the presence of foreign species, instead, can be ascribed to surface modifications, as confirmed by TEM analyses.

The nitrogen adsorption-desorption isotherms (Figure 2) corresponded to Type IV isotherm[61] and showed a hysteresis loop of H4 type, with the two branches almost horizontal and parallel over a wide range of p/p° for the samples TiO_2, Pt-TiO_2 and Pt-TiO_2-N0.5, while for the sample Pt-TiO_2-W0.5 the hysteresis loop is intermediate between the types H3 and H4. These results suggest that the appearance of the hysteresis loop is more probably due to agglomeration of the particles, although also pores smaller than 100 Å have been identified by the size distribution analysis for the samples containing W.

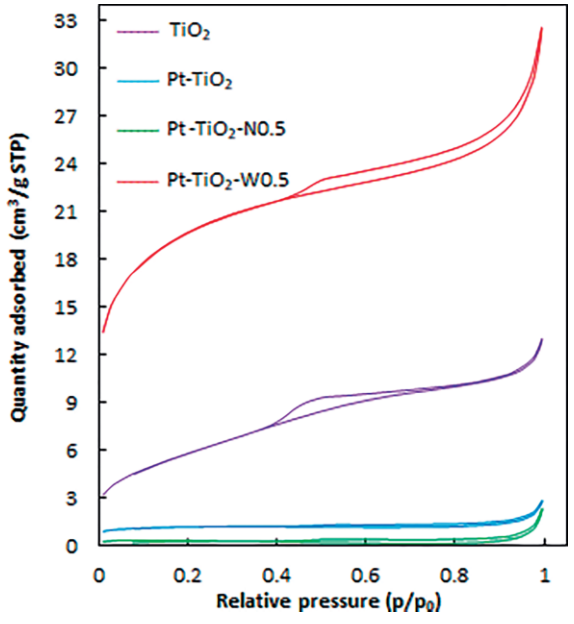

Figure 2. N_2 adsorption-desorption isotherms of some representative samples.

TEM micrographs of the bare TiO_2 sample (Figure 3A–B) show the typical morphology of rutile nanoparticles: cluster of elongated rod-like particles with sharp borders and length of some tens of nanometers.

By adding platinum (sample Pt-TiO_2 Figure 3C–D) the morphology becomes quite different: clusters become bigger, consisting of more particles. Notably, the shape of the single particles changes significantly, becoming almost round with diameter less than 10 nm.

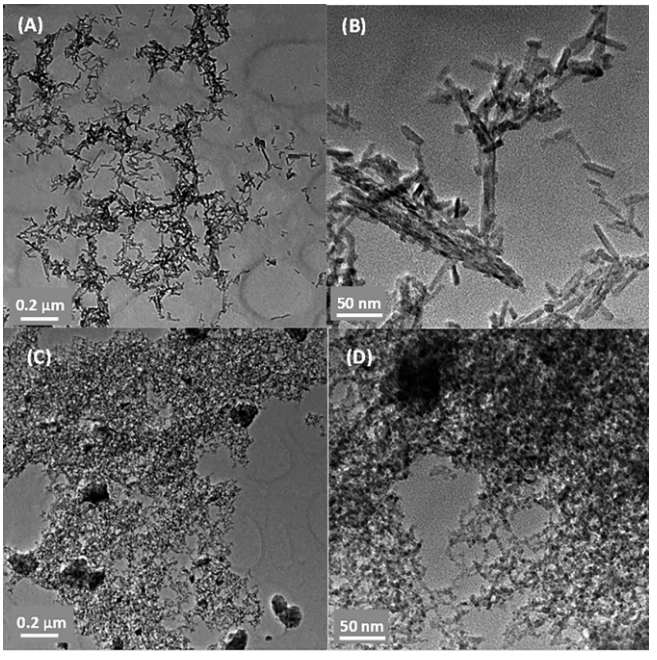

Figure 3. TEM micrographs of the bare TiO_2 sample at 10000x (A) and 50000x (B) magnifications and of Pt-TiO_2 sample at 10000x (C) and 50000x (D) magnifications.

A situation even more different was observed for the powders containing N or W. The sample Pt-TiO_2-N0.5, for instance, shows the presence of strange long needle-like particles (Figure 4A–B) whilst big and thick particles with irregular shape, whose dimension range from few tens up to hundreds of manometers, can be noticed for the Pt-TiO_2-W0.5 sample (Figure 4 C–D).

These results indicate that the different dopants influenced also the morphology of the samples.

In Figure 4(E–F) the sample Pt-TiO_2-W0.25 before (E) and after (F) its use in photocatalytic runs is shown. After the photocatalytic test no significant differences of shape and dimension of the particles can be noticed, but the clusters appear slightly bigger (Figure 4F), due to some aggregation which took place during the run.

High Resolution TEM (HR-TEM) and selected area electron diffraction (SAED) analysis of sample Pt-TiO_2-W0.25 (Figure 5) show that the obtained rutile is well crystallized with clear parallel lattice fringes. The fringe spacing is approximately 0.32 nm, which correspond to the (1 1 0) lattice spacing of rutile TiO_2.[62]

In the inset of Figure 5 a sharper image (processed through an Inverse Fast Fourier Transform) of the highlighted area and the histogram showing the exact calculation of d-space are reported. Moreover, HR-TEM micrographs confirm that the crystalline structure did not change after the catalytic test.

In Figure 6 the reflectance spectra of bare TiO_2, Pt-TiO_2, Pt-TiO_2-N and Pt-TiO_2-W samples are reported. In the presence of Pt an increase of the absorption in the visible light region, with respect to the bare TiO_2, occurred, whilst a slight decrease was observed in the presence of nitrogen. The light absorption above 500 nm of the Pt-TiO_2-N and Pt-TiO_2-W samples can be attributed to oxygen vacancies, in accordance with the litera-

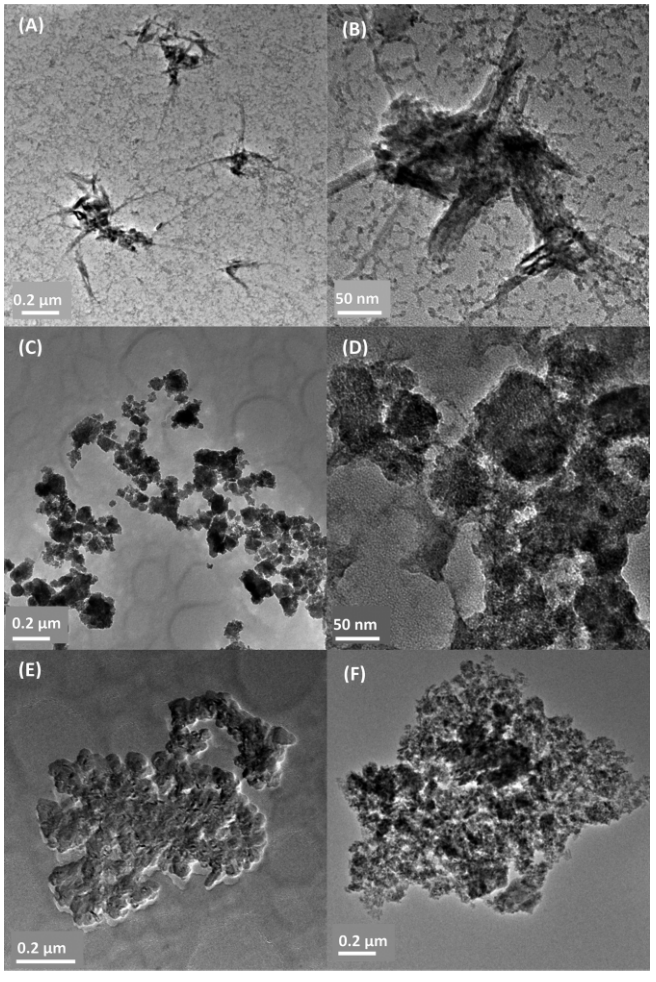

Figure 4. TEM micrographs of the samples Pt-TiO_2-N0.5 (A and B), Pt-TiO_2-W0.5 (C and D) and Pt-TiO_2-W0.25 before (E) and after (F) the photocatalytic runs.

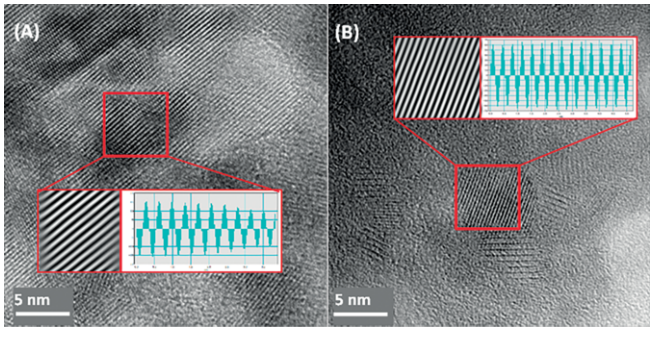

Figure 5. High resolution TEM images of the sample Pt-TiO_2-W0.25 before (A) and after (B) the photocatalytic runs. Inset: processed image of highlighted area and plot profile of atomic fringe showing the calculations of d-spacing.

ture.[63,64] In Figure 6B it can be noticed that the spectrum of Pt-TiO_2 is red shifted with respect to those of the samples containing W because the sample mainly consists of rutile phase. Tungsten stabilized the anatase phase,[65] its presence blue shifted the absorbance of the samples and increased the percentage of reflectance. The band gap values (Table 1) were obtained by extrapolating a linear fitting in the Tauc plot diagram (Figure 7). Bare TiO_2 exhibited a band gap of 2.98 eV which is typical of the rutile polymorph, reduced to 2.90 eV after Pt adding. A progressive decrease of the band gap values was observed (Table 1) at increasing nitrogen amount. This is probably due to a broadening of the valence band following the hybridization of the O *2p* states with the N *2p* states, with a consequent upward shift of the valence band maximum. In the presence of tungsten there was a band-gap increase, with the exception of the samples with the highest tungsten percentages and the Pt-TiO_2-N0.5W0.5 sample for which a decrease of the band-gap occurred. The band bap increase in the samples containing W can be attributed to the formation of the anatase phase (the band gap of anatase is higher than that of rutile) whose quantity rises with the W amount. For the highest W percentage two phenomena can take place which contribute in opposite way to the band gap value: the increase of the anatase fraction and the shift towards higher potential values of the CB edge with the W amount.[66] As reported in Table 1,

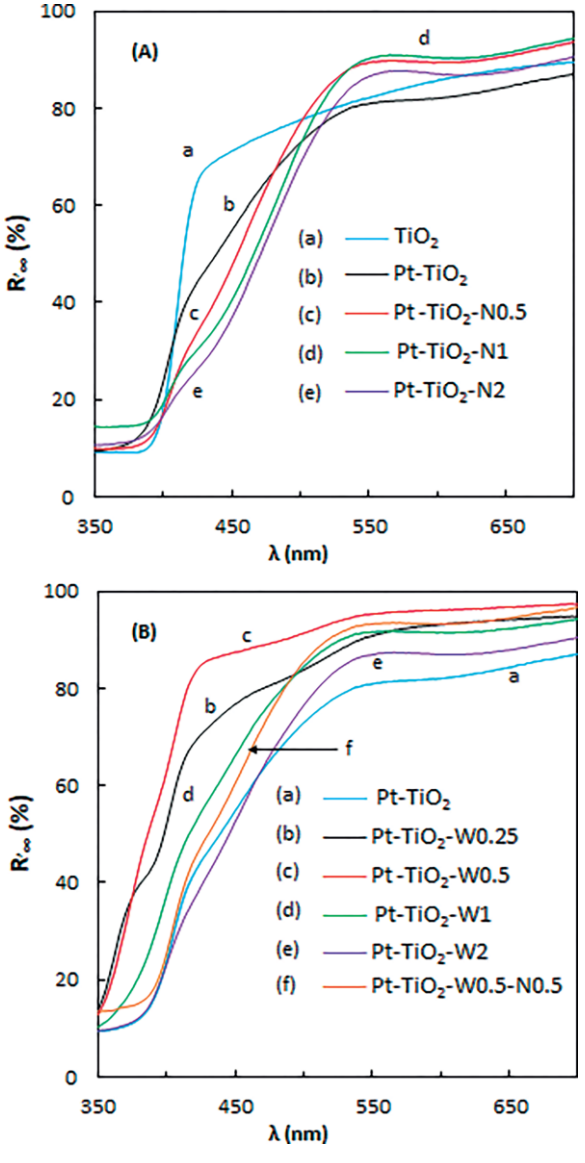

Figure 6. DRS spectra of the various photocatalysts.

indeed, there is a progressive band gap reduction with increasing tungsten percentage despite the increased quantity of anatase. The presence of surface oxygen vacancies in the doped samples could also play a role in determining the band gap value.

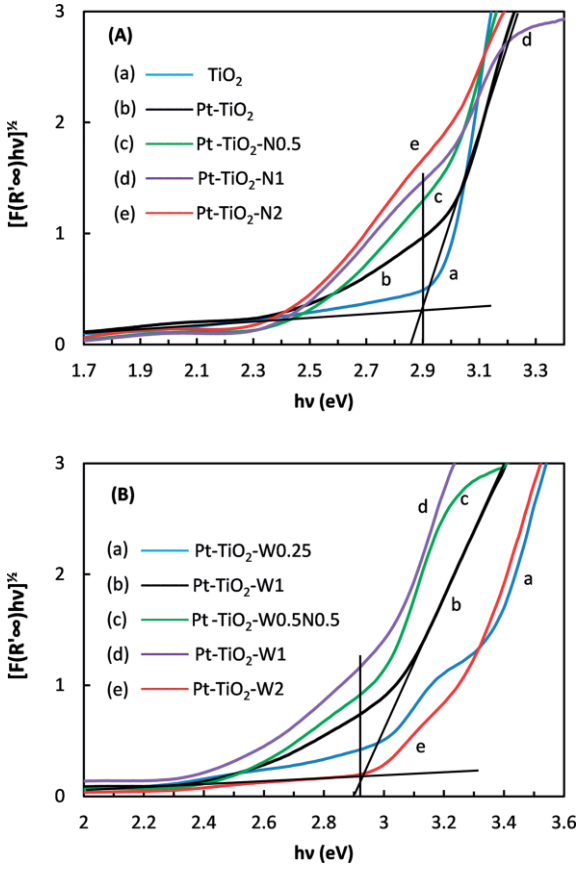

Figure 7. Tauc plot diagram of the various photocatalysts.

The spectra of the TiO_2 and Pt-TiO_2 samples exhibited a single sharp edge while those of the doped samples showed two linear sections, being the second attributable to the existence of a mid-gap band located above the valence band[42,64] or below the conduction band, due to the additional energy levels created by the doping agents.

2.2 Photocatalytic Runs

No formation of H_2 occurred in the presence of bare TiO_2, confirming the essential role of Pt. The results of the photocatalytic runs carried out under UV light irradiation in the presence of Pt-TiO_2, Pt-TiO_2-N0.5, and Pt-TiO_2-W0.5 samples are reported in Figure 8. Concentration of glucose and its partial oxidation products in liquid phase, along with H_2 and CO_2 in gas phase, vs. irradiation time are reported in Figure 8A–C whilst the amounts of H_2 and CO_2 per gram of catalyst obtained after 6 h of irradiation are reported in Figure 8D. Notably, no CO and/or CH_4 were detected under the experimental conditions used. Arabinose, erythrose and formic acid were the main observed species deriving from the partial glucose oxidation, according to previous results.[22]

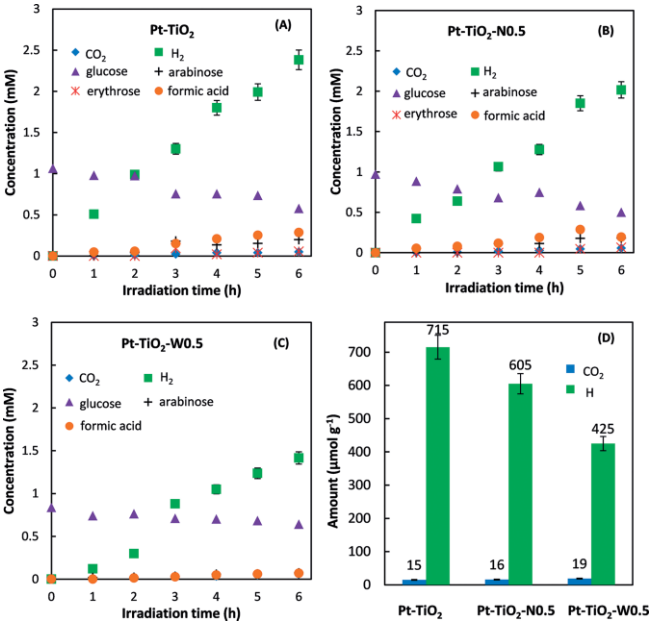

Figure 8. Concentration of: (Violet triangle) glucose, (Black cross) arabinose, (Red star) erythrose and (Orange ball) formic acid in liquid phase and (Blue diamond) CO_2, (Green square) H_2 in gas phase, vs. irradiation time under UV light irradiation in the presence of some photocatalysts (A–C) and amounts of H_2 and CO_2 per gram of catalyst after 6 h of irradiation (D). The error of analysis is less than ±5.

In Table 2 the glucose conversion and the selectivity towards the different by-products are reported. After 6 h of UV irradiation the substrate conversion was 45.8 % by using the Pt-TiO_2 sample, a small increase was obtained by adding 0.5 % of nitrogen, and a significant reduction was observed in the presence of 0.5 % of tungsten. With regard to the selectivity towards arabinose, no great variation was observed in the presence of the three samples; the selectivity to formic acid was reduced by the presence of foreign elements, and a difference was obtained in the distribution of the oxidation products. In particular, no erythrose was detected in the presence of the Pt-TiO_2-W0.5 sample. The results confirm that glucose oxidation occurred with the C1–C2 break, following the mechanism reported in Figure 9, in accordance with literature.[19,22] The highest H_2 production (715 μmol g^{-1} after 6 h of irradiation, Figure 8D) was measured with the non-doped sample and both N and W caused a decrease, obtaining the lowest amount with the addition of W. Similar CO_2 amounts were detected in the presence of the three samples.

Table 2. Glucose conversion (X) and selectivity (S) to arabinose, erythrose and formic acid after 6 h of UV irradiation.

Sample	$X_{glucose}$	$S_{arabinose}$	$S_{erythrose}$	$S_{formic\ acid}$
Pt-TiO_2	45.8	40.7	11.4	58.6
Pt-TiO_2-N0.5	48.4	38.3	13.6	41.1
Pt-TiO_2-W0.5	23.3	36.4	–	35.5

In Figure 10 the trend of the concentration of all of the species measured during the photocatalytic runs carried out under a halogen lamp irradiation in the presence of the different samples is reported. The amount of both CO_2 and H_2 increased

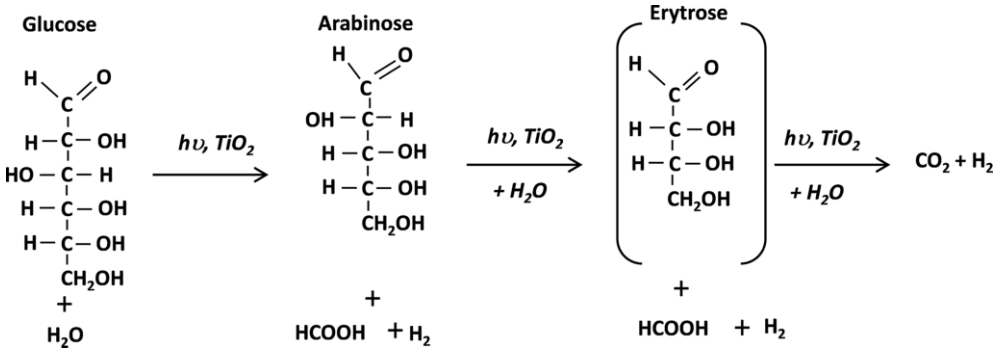

Figure 9. Hypothesized oxidation path of glucose.

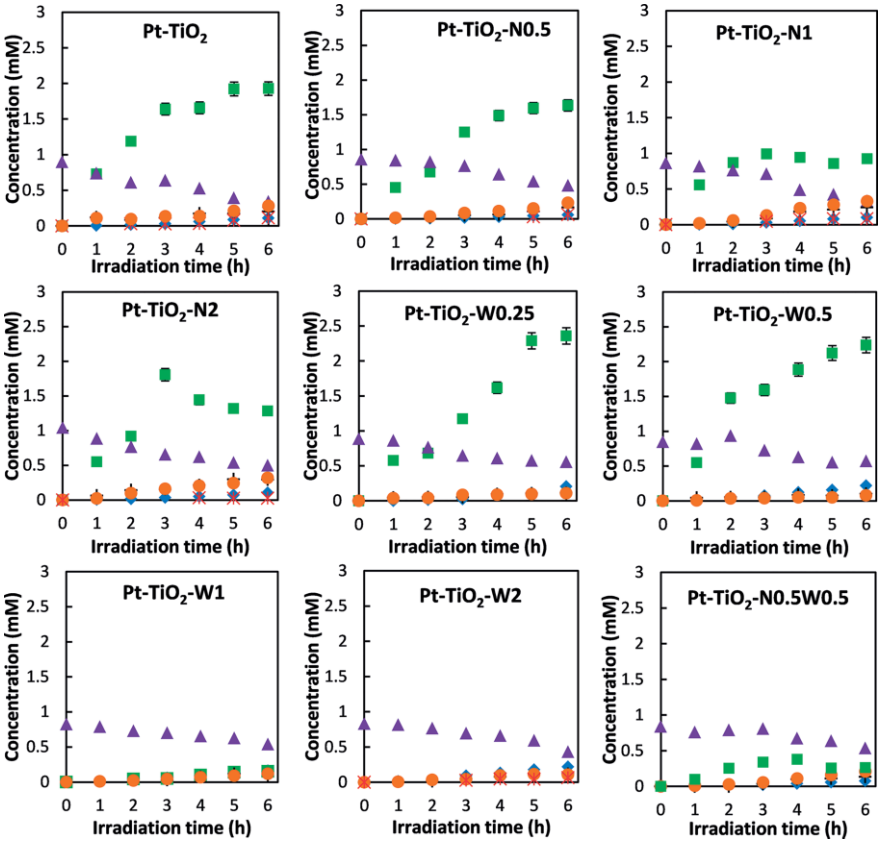

Figure 10. Concentration of: (Violet triange) glucose, (Black cross) arabinose, (Red star) erythrose, (Orange ball) formic acid in liquid phase, (Blue diamond) CO_2, (Green square) H_2 in gas phase, vs. irradiation time under HL irradiation. The error of analysis is less than ±5.

as the glucose concentration decreased. Glucose oxidation can occur via direct hole transfer to glucose bound to TiO_2 surface, due to the strong adsorption of the substrate, as reported in literature.[67–70] Photooxidation of carbohydrates in water was reported to involve sequential cleavage of formic acid to form the shorter aldose and H_2. The most active samples for H_2 production where those containing the lowest W percentages.

In Table 3 the glucose conversion and the selectivity to arabinose, erythrose and formic acid after 6 h of HL irradiation are reported. The behaviour of powders for glucose degradation was similar to that observed under UV light irradiation and the same oxidation products were obtained. The results showed that the photocatalytic glucose degradation mechanism is the same, regardless of the irradiation source used. In the presence of N-doped catalysts, the glucose conversion was very similar or slightly lower than that measured by using Pt-TiO_2, exhibiting the different N-doped samples a bell shaped trend of the photocatalytic efficiency. A noticeable negative effect, instead, was observed in the presence of W-doped catalyst, being the lowest value obtained by using the Pt-TiO_2-W0.5 catalyst. By adding N, the selectivity to arabinose and formic acid was higher than that found in the presence of the Pt-TiO_2 samples for all of the dopant percentages, whilst a bell shaped behaviour was observed by increasing the W dopant amount. The selectivity to erythrose was low and negligible in the presence of N and W, respectively, with the exception of the sample Pt-TiO_2-W2.

Table 3. Glucose conversion, selectivity to arabinose, erythrose and formic acid and amounts of CO_2 and H_2 per grams of catalyst after 6 h of HL irradiation.

Sample	$X_{glucose}$	$S_{arabinose}$	$S_{erythrose}$	$S_{formic\ acid}$	CO_2 [μmol g^{-1}]	H_2 [μmol g^{-1}]
Pt-TiO_2	62.1	35.9	20.1	49.9	33	578
Pt-TiO_2-N0.5	43.7	44.0	16.4	61.4	18	491
Pt-TiO_2-N1	61.3	45.9	16.0	61.8	30	278
Pt-TiO_2-N2	51.9	54.3	4.7	58.4	31	385
Pt-TiO_2-W0.25	37.4	33.5	–	32.3	85	708
Pt-TiO_2-W0.5	32.5	36.7	–	28.6	66	671
Pt-TiO_2-W1	34.5	41.5	–	41.5	49	45
Pt-TiO_2-W2	48.1	28.9	15.8	26.8	65	–
Pt-TiO_2-N0.5W0.5	36.1	44.5	–	68.7	23	79

This behaviour indicates the occurrence of a different glucose reaction mechanism in the presence of the various photocatalysts,[22] due to different effects of the foreign species (which is not easy to fully explain) on the surface properties. The glucose conversion in the presence of the co-doped sample was similar to that observed in the presence of the Pt-TiO_2-W samples. Notably, no improvement was noticed with respect to the Pt-TiO_2 sample.

In Figure 11 the amounts of H_2 and CO_2 after 6 h of HL irradiation are reported. A negative effect for H_2 and CO_2 formation with respect to the Pt-TiO_2 sample was noticed in the presence of nitrogen whilst an increase of the formation of both products was observed by using low amounts of tungsten, despite the lower glucose conversion (Table 3) compared to that obtained with the N-doped samples. The highest W amounts had a detrimental effect on the phototocatalytic H_2 production, being the latter negligible and equal to 708 μmol g^{-1} by using the Pt-TiO_2-W2 and Pt-TiO_2-W0.25 samples, respectively. H_2 evolution was low also when the co-doped Pt-TiO_2-N0.5W0.5 catalyst was employed. By comparing the amounts of CO_2 produced under UV irradiation with those obtained under HL irradiation, in the latter a general more significant mineralization was obtained with a maximum in the presence of Pt-TiO_2-W0.25 sample. The finding that the activity of the co-doped sample was not higher than that of the corresponding single doped samples, indicates that there was not a synergistic effect between the two dopant species, and probably the high defects number favoured the e^-/h^+ recombination.

In order the reduction of H^+ to H_2 take place, it is necessary that the conduction band level of the photocatalyst is more negative than the potential of the H^+/H_2 couple ($E_{H+/H2}$ = 0 V vs. NHE at pH = 0) (Figure 12). Generally, the TiO_2 rutile CB edge has a slight negative value,[71] and it is reported that the presence of N in TiO_2 causes a VB shift towards less positive values whilst the incorporation of W induces a CB shift towards less negative values.[66] These considerations could justify the drop in H_2 production by using the W-doped samples for the highest metal amounts. It is worth noticing that the value of

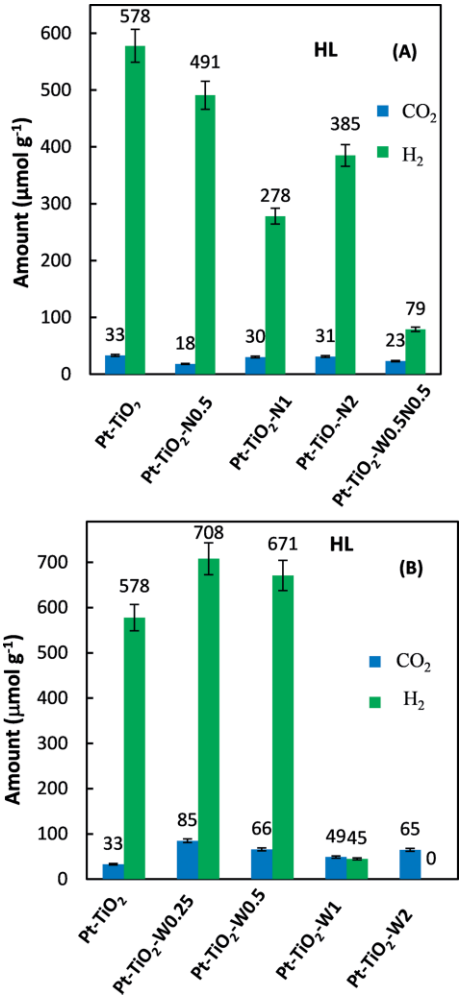

Figure 11. CO_2 and H_2 amount per gram of catalyst after 6 h of HL irradiation. The error of analysis is less than ±5.

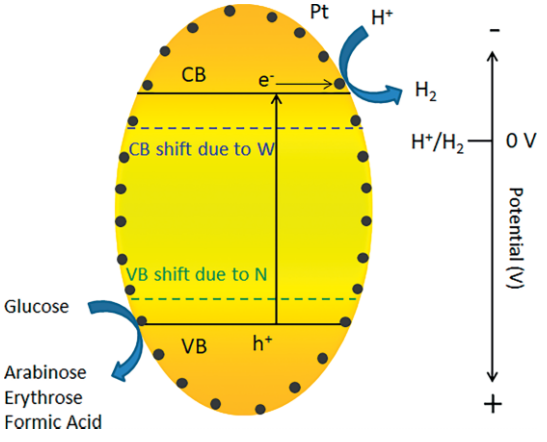

Figure 12. Photocatalytic hypothesized mechanism of glucose oxidation and H_2 production.

the edge of the conduction band progressively moves to less negative values as the amount of tungsten increases, reaching values very close to the hydrogen reduction potential. In Table 4 the energy values of the conduction band (E_{CB}) and valence band (E_{VB}) edges, calculated in accordance with Xu and Schoonen,[72] are reported. The values were calculated by the empirical Equation (1) and Equation (2):[73]

$$E_{CB} = \chi - E^e - 0.5\ E_g \quad (1)$$

$$E_{VB} = E_{CB} + E_g \quad (2)$$

Table 4. Energy values of the conduction band (E_{CB}) and valence band (E_{VB}) edges.

Sample	E_{CB} [eV]	E_{VB} [eV]
Pt-TiO_2-W0.25	–0.29	2.97
Pt-TiO_2-W0.5	–0.24	2.92
Pt-TiO_2-W1	–0.12	2.80
Pt-TiO_2-W2	–0.09	2.77

where E_g is the band gap, E^e is the energy of free electrons vs. hydrogen (4.5 eV), and χ is the electronegativity of the semiconductor, calculated as the geometric mean of Mulliken's electronegativities of the constituent atoms. For TiO_2 χ is 5.84 eV.[72] Even if absolute values cannot be obtained by means of this method because the structural factors are not taken into account, it can provide a rough estimation and a trend of the relative energy of CB and VB vs. normal hydrogen electrode (NHE). By increasing the W amount, a progressive decrease of the CB edge was estimated (Table 4), and for the sample Pt-TiO_2-W2 the value is very close to 0 V. This can justify the inactivity of this sample for H_2 production.

Some of the synthesized samples were also tested under natural solar light irradiation for 3.5 h. Figure 13 reports the reactivity results obtained by using Pt-TiO_2 and Pt-TiO_2-W0.25 samples, chosen as the most representative ones, vs. the cumulative irradiation energy. Both samples were more active under natural solar light irradiation than under HL irradiation, and the increase of activity was higher in the presence of the Pt-TiO_2-W0.25 sample, being the highest H_2 production equal to 3770 μmol g^{-1} under natural solar light irradiation (Figure 13B). The above results showed the positive effect of tungsten on the H_2 formation by using the solar energy.

By comparing the photoactivity of Pt-TiO_2 and Pt-TiO_2-W0.25 samples under natural solar light irradiation and at the same cumulative energy value (Table 5), a higher glucose conversion and H_2 and CO_2 production can be noticed in the presence of tungsten. This finding indicates the beneficial role of W in the activation of TiO_2 for H_2 production by using the solar irradiation.

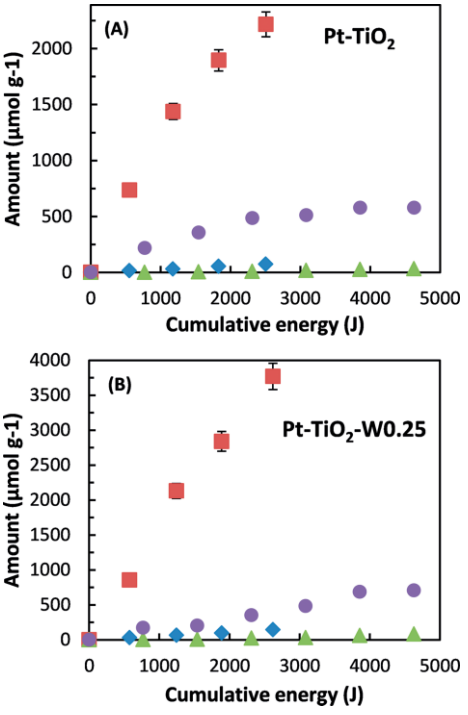

Figure 13. Amounts of CO_2 and H_2 per gram of catalyst under SOL or HL irradiation in the presence of: Pt-TiO_2 (A) and Pt-TiO_2-W0.25 (B) samples; (Blue diamond) CO_2 SOL, (Red square) H_2 SOL, (Green triangle) CO_2 HL, (Violet ball) H_2 HL. The error of analysis is less than ±5.

The results found are in accord with those reported in the literature.[16] Many papers report the H_2 production from glucose photoreforming[16] in the presence of different types of TiO_2 doped materials and by using Xe, Hg, UVA, UV LED, and solar simulating lamps as the light sources. By using a solar light simulator, Kondarides et al.[74] observed H_2 production rates equal to 2.4 mmol $gcat^{-1}$ h^{-1} in the presence of Pt-TiO_2 (P25) with the complete mineralization of glucose to CO_2 and without the formation of high value-added products. By using a 350 W Xe lamp as the irradiation source, 6.7 mmol $gcat^{-1}$ h^{-1} of H_2 were obtained over Pt/TiO_2 nanosheets (Pt 2 %) with exposed the {001} facet.[75] Pd_{shell}–Au_{core} nanoparticles immobilized on TiO_2 exhibited a high efficiency for H_2 production under UV irradiation (8.8 mmol $gcat^{-1}$ h^{-1}).[76] To the best of our knowledge no data about the activity under natural solar light irradiation are reported in literature. In our system the best H_2 production rates was ca. 1.0 mmol $gcat^{-1}$ h^{-1} by using Pt-TiO_2-W0.25 under natural solar irradiation.

Some runs were carried out under HL irradiation by using, instead of glucose, formic acid (initial concentration 1 mM) as the sacrificial reagent, due to the simplicity of this molecule and the direct conversion to CO_2 and H_2, in accordance with

Table 5. Glucose conversion (X), selectivity (S) to arabinose, erythrose, formic acid, and amounts of CO_2 and H_2 per gram of catalyst under natural solar irradiation at the same cumulative energy value (2500 J).

Sample	$X_{glucose}$	$S_{arabinose}$	$S_{erythrose}$	$S_{formic\ acid}$	CO_2 [μmol g^{-1}]	H_2 [μmol g^{-1}]
Pt-TiO_2	64.40	49.96	25.54	67.63	74	2218
Pt-TiO_2-W0.25	81.47	17.62	0.00	13.48	135	3734

literature.[77,78] The evaluation of the stoichiometric ratio between the initial amount of formic acid and formed hydrogen allowed to indirectly hypothesize the occurrence of water splitting. Indeed, the amount of H_2 produced was higher than that which would have been derived simply from formic acid.

The substrate was completely degraded after 2 h of irradiation; afterwards the CO_2 concentration remained constant whilst the amount of H_2 began to decrease. The H_2 maximum production was ca. 1160 μmol (corresponding to 1449 μmol g^{-1}), almost 1.5 times greater than the formic acid initial molar quantity, whilst the CO_2 amount was a little lower than the stoichiometric value. This finding can be explained by considering that a fraction of formed CO_2 remained probably dissolved in water and/or adsorbed on the photocatalyst surface. By considering the formic acid decomposition (dehydrogenation) reaction[77,78] according to Equation (3):

$$HCOOH \rightarrow CO_2 + H_2 \quad (3)$$

The finding that the molar ratio between H_2 and CO_2 was higher than 1 and that the H_2 amount was higher than that corresponding to the total mineralization of formic acid, suggests that the produced H_2 derived from both formic acid and water splitting, with the simultaneous formation of O_2. Moreover, the decrease of the H_2 amount after formic acid disappearance was probably due to the occurrence of the back reaction between H_2 and O_2 and/or to the Ti^{4+} reduction by H_2. Probably, the former reaction occurred also during the first hours of irradiation, but its rate increased by increasing the quantity of O_2 formed and present in the solution. When the substrate was still present, the amount of H_2 that recombined with oxygen was balanced by that coming from formic acid. This explains the observed decrease of H_2 production reaction rate by increasing the irradiation time, until an almost constant value or a decrease of its concentration was reached (Figure 14). Notably, no production of H_2 was observed in the absence of formic acid, confirming the essential role of the sacrificial agents in the electron/hole separation. Some of these considerations based on the experimental results could also be extended to the H_2 production from glucose, because also in this case a decrease of the evolution rate of H_2 over time was noticed. Nevertheless, it was not possible to rationalize these findings or to check a mass balance as glucose was not completely mineralized, and other valuable products were obtained from its transformation.

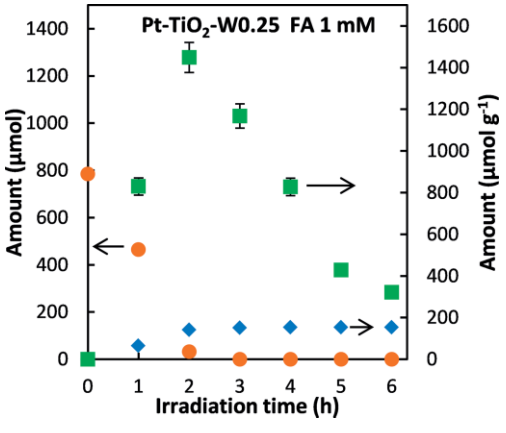

Figure 14. Concentration of: (Orange ball) formic acid, (Blue diamond) CO_2 and (Green square) H_2 vs. time under HL irradiation in the presence Pt-TiO_2-W0.25 sample. The error of analysis is less than ±5.

3. Conclusions

N and/or W doped Pt-TiO_2 samples were used for the anaerobic glucose photo-conversion in aqueous solution under a halogen lamp and natural solar light irradiation with the dual purpose of obtaining high value-added products from the partial oxidation of the substrate and H_2 from the photo-reforming process. Different results were obtained in the presence of the two dopant species evidencing a different influence on the properties of TiO_2. The presence of N in the Pt-TiO_2 sample generally did not influence the glucose conversion but increased the selectivity to arabinose and formic acid and decreased the H_2 production. Tungsten had a negative effect on the substrate conversion and a beneficial role on the H_2 evolution, with the exception of the highest dopant amounts. Moreover, arabinose, erythrose and formic acid were the main products of the partial oxidation of glucose when using the N-doped samples, whilst erythrose was found in the presence of W only for the highest dopant amount. These findings can be attributed to different TiO_2 surface properties when N and W are present. Moreover, also a difference in the electronic properties was observed in the presence of the two different dopants, in particular, N caused a VB shift towards less positive values whilst W induced a CB shift towards less negative values. The photocatalysts showed a good activity for H_2 production also under direct solar light irradiation, demonstrating the applicability of this type of materials under real-life conditions.

4. Experimental Section

4.1 Photocatalysts Preparation: Bare TiO_2 powders were prepared by adding 10 mL of $TiCl_4$ (Sigma–Aldrich) to 40 mL of distilled water at room temperature. After ca. 20 min of stirring, the clear solution was placed in a Teflon-lined stainless steel autoclave at room temperature, and afterwards heated at 100 °C for 48 h. The solid was recovered by drying at 60 °C, and it was named TiO_2. Pt-TiO_2 samples (nominal Pt weight percentage 0.5 %) were obtained by adding the proper amount of $PtCl_4$ (Sigma–Aldrich) to the $TiCl_4/H_2O$ solution prior to the hydrothermal treatment. Pt-Nitrogen, Pt-Tungsten or Pt-Nitrogen-Tungsten loading were performed under mild conditions: appropriate amounts of NH_4Cl and WCl_6 were added to the clear Pt-$TiCl_4/H_2O$ solution to obtain samples containing different weight percentages of N and W during the hydrothermal treatment. The samples were indicated as: Pt-TiO_2-N0.5, Pt-TiO_2-N1, Pt-TiO_2-N2, Pt-TiO_2-W0.25, Pt-TiO_2-W0.5, Pt-TiO_2-W1, Pt-TiO_2-W2, Pt-TiO_2-N0.5W0.5, the figures indicating the weight percentages of N and/or W.

4.2 Characterization of the Samples: X-ray diffraction (XRD) patterns of the powders were obtained by a PANalytical X'pertPro X-ray diffractometer with Cu-K_α radiation and 2θ scan rate of 2 °C/min. The crystalline sizes of the samples were determined by using the Scherrer equation. The diffuse reflectance spectra (DRS) in the 250–800 nm wavelength range were obtained by using a Shimadzu

UV-2401 PC spectrophotometer with $BaSO_4$ as the reference material. Band gap values were determined by plotting the modified Kubelka–Munk function, $[F(R'_\infty)h\nu]^{1/2}$, vs. the energy of the exciting light. The specific surface area (SSA) and the pore size distribution (PSD) of the photocatalysts were determined by nitrogen adsorption-desorption measurements with a Micromeritics ASAP 2020 apparatus. SSA's were calculated by the BET equation in the p/po interval 0.05–0.33 while the PSD's were calculated by using the Barrett Joyner Halenda (BJH) methods.

Transmission electron microscopy (TEM) measurements were carried out by a JEOL (Japan) JEM-2100 electron microscope operating at 200 KV, while HR-TEM images SAED (Selected Area Electron Diffraction) patterns were obtained by a Gatan (USA) MSC camera. Samples were prepared by dispersing them in 2 mL of deionized water and by sonicating them for 5 minutes. A drop of each dispersion was spread on a copper holey carbon coated grid and dried overnight prior TEM analysis. Particles size and atomic layers spacing were measured by Gatan (USA) Digital Micrograph software.

4.3 Photocatalytic Activity: Some preliminary runs were carried out under UV light (by using a 125 W medium pressure Hg lamp) to test the efficiency of the catalysts. The lamp radiant power, measured by a radiometer Delta Ohm DO9721, was ca. 120 W m^{-2} in the range 315–400 nm. Successively, all the prepared samples were tested in a 1040 mL Pyrex cylindrical reactor illuminated by a 150 W halogen lamp axially immersed within the photoreactor which was filled with 800 mL of 1 mM glucose solution. The lamp radiant power was ca. 2100 W m^{-2} in the 450–750 nm range, and 17 W m^{-2} in the range 315–400 nm. N_2 was bubbled into suspensions for ca. 0.5 h under dark to remove O_2 from the solution, then the reactor was sealed and the lamp switched on for 6 h. The best photocatalysts were tested also under natural solar light irradiation by using a closed batch Pyrex reactor whose volume was 250 mL, filled with 100 mL of glucose solution. In all cases, the amount of catalyst used was 1.0 g L^{-1} of suspension. The runs under natural solar light irradiation lasted 3.5 h. Glucose was used both as sacrificial agent for H_2 production and as reagent to obtain high value chemicals from its partial oxidation. For the sake of comparison some experiments were performed by using formic acid instead of glucose. The concentrations of glucose, photo-products and formic acid were measured by a Thermo Scientific Dionex UltiMate 3000 HPLC equipped with a Diode Array and a refractive index detectors equipped with a REZEK ROA Organic acid H^+ column. An aqueous 2.5 mM H_2SO_4 solution was used as the eluent at a flow rate of 0.6 mL min^{-1}. The gaseous H_2 and CO_2 species were analyzed by a HP 6890 Series GC System equipped with a Supelco GC 60/80 Carboxen™-1000 packed column and a thermal conductivity detector (TCD). Helium was used as the carrier gas. The error of analysis was less than ±5 %.

Keywords: Photocatalysis · Doping · Titanium dioxide · Glucose reforming · Hydrogen evolution · Oxidation

[1] J. D. Holladay, J. Hu, D. L. King, Y. Wang, *Catal. Today* **2009**, *139*, 244.
[2] S. E. Hosseini, M. A. Wahid, *Renewable Sustainable Energy Rev.* **2016**, *57*, 850.
[3] K. Mazloomi, C. Gomes, *Renewable Sustainable Energy Rev.* **2012**, *16*, 3024.
[4] N. Florin, A. Harris, *Environmentalist* **2007**, *27*, 207.
[5] R. M. Navarro, M. C. Sánchez-Sánchez, M. C. Alvarez-Galvan, F. del Valle, J. L. G. Fierro, *Energy Environ. Sci.* **2009**, *2*, 35.
[6] N. Meng, D. Y. C. Leung, M. K. H. Leung, K. Sumathy, *Fuel Process. Technol.* **2006**, *87*, 461.
[7] R. Li, *Chinese J. Catal.* **2017**, *38*, 5.
[8] K. Maeda, K. Domen, *J. Phys. Chem. Lett.* **2010**, *1*, 2655.
[9] R. Kothari, D. Buddhi, R. L. Sawhney, *Renewable Sustainable Energy Rev.* **2008**, *12*, 553.
[10] J. Zhu, M. Zäch, *Curr. Opin. Colloid Interface Sci.* **2009**, *14*, 260.
[11] H. Bahruji, M. Bowker, P. R. Davies, L. S. Al-Mazroai, A. Dickinson, J. Greaves, D. James, L. Millard, F. Pedrono, *J. Photochem. Photobiol. A* **2010**, *216*, 115.
[12] M. Ni, M. K. H. Leung, D. Y. C. Leung, K. Sumathy, *Renewable Sustainable Energy Rev.* **2007**, *11*, 401.
[13] D. I. Kondarides, V. M. Daskalaki, A. Patsoura, X. E. Verykios, *Catal. Lett.* **2008**, *122*, 26.
[14] M. de Oliveira Melo, L. Almeida Silva, *J. Braz. Chem. Soc.* **2011**, *22*, 1399.
[15] X. Fu, J. Long, X. Wang, D. Y. C. Leung, Z. Ding, L. Wu, Z. Zhang, Z. Li, X. Fu, *Int. J. Hydrogen Energy* **2008**, *33*, 6484.
[16] A. Puga, *Coord. Chem. Rev.* **2016**, *315*, 1.
[17] M. F. Kuehnel, E. Reisner, *Angew. Chem. Int. Ed.* **2018**, *57*, 3290.
[18] J. C. Colmenares, A. Magdziarz, A. Bielejewska, *Bioresour. Technol.* **2011**, *102*, 11254.
[19] R. Chong, J. Li, Y. Ma, B. Zhang, H. Han, C. Li, *J. Catal.* **2014**, *314*, 101.
[20] M. Bellardita, E. I. García-López, G. Marcì, B. Megna, F. R. Pomilla, L. Palmisano, *RSC Adv.* **2015**, *5*, 59037.
[21] W. Deng, Q. Zhang, Y. Wang, *Catal. Today* **2014**, *234*, 31.
[22] M. Bellardita, E. García-López, G. Marcì, L. Palmisano, *Int. J. Hydrogen Energy* **2016**, *41*, 5934.
[23] T. Montini, M. Monai, A. Beltram, I. Romero-Ocaña, P. Fornasiero, *Mater. Sci. Semicon. Proc.* **2016**, *42*, 122.
[24] H. Dong, G. Zeng, L. Tang, C. Fan, C. Zhang, X. He, Y. He, *Water Res.* **2015**, *79*, 128.
[25] D. Dvoranová, V. Brezová, M. Mazúr, M. A. Malati, *Appl. Catal. B* **2002**, *37*, 91.
[26] A. Di Paola, E. García-López, S. Ikeda, G. Marcı`, B. Ohtani, L. Palmisano, *Catal. Today* **2002**, *75*, 87.
[27] J. Choi, H. Park, M. R. Hoffmann, *J. Phys. Chem. C* **2010**, *114*, 783.
[28] L. Gomathi Devi, R. Kavitha, *Appl. Catal. B* **2013**, *140–141*, 559.
[29] R. Asahi, T. Morikawa, H. Irie, T. Ohwaki, *Chem. Rev.* **2014**, *114*, 9824.
[30] R. Amadelli, L. Samiolo, M. Borsa, M. Bellardita, L. Palmisano, *Catal. Today* **2013**, *206*, 19.
[31] J. Belošević-Cavor, K. Batalović, V. Koteski, J. Radaković, C. M. Rangel, *Int. J. Hydrogen Energy* **2015**, *40*, 9696.
[32] B. Choudhury, B. Borah, A. Choudhury, *Mater. Sci. Eng. B* **2013**, *178*, 239.
[33] A. Kubacka, B. Bachiller-Baeza, G. Colón, M. Fernández-García, *Appl. Catal. B* **2010**, *93*, 274.
[34] W. M. Campbell, A. K. Burrell, D. L. Officer, K. W. Jolley, *Coord. Chem. Rev.* **2004**, *248*, 1363.
[35] T. Wu, G. Liu, J. Zhao, H. Hidaka, N. Serpone, *J. Phys. Chem. B* **1998**, *102*, 5845.
[36] R. Fiorenza, M. Bellardita, S. Scirè, L. Palmisano, *Catal. Today* https://doi.org/ttps://doi.org/10.1016/j.cattod.2017.12.011, **2018**.
[37] G. Longo, F. Fresno, S. Gross, U. L. Štangar, *Environ. Sci. Pollut. Res.* **2014**, *21*, 11189.
[38] D. P. Kumar, M. V. Shankar, M. M. Kumari, G. Sadanandam, B. Srinivas, V. Durgakumari, *Chem. Commun.* **2013**, *49*, 9443.
[39] L. Chen, X. Zhou, B. Jin, J. Luo, X. Xu, L. Zhang, Y. Hong, *Int. J. Hydrogen Energy* **2016**, *41*, 7292.
[40] R. Asahi, T. Morikawa, T. Ohwaki, K. Aoki, Y. Taga, *Science* **2001**, *293*, 269.
[41] S. A. Ansari, M. M. Khan, M. O. Ansari, M. H. Cho, *New J. Chem.* **2016**, *40*, 3000.
[42] M. Bellardita, M. Addamo, A. Di Paola, L. Palmisano, A. M. Venezia, *Phys. Chem. Chem. Phys.* **2009**, *11*, 4084.
[43] H. Irie, Y. Watanabe, K. Hashimoto, *J. Phys. Chem. B* **2003**, *107*, 5483.
[44] N. Serpone, *J. Phys. Chem. B* **2006**, *110*, 24287.
[45] M. Ilie, B. Cojocaru, V. I. Parvulescu, H. Garcia, *Int. J. Hydrogen Energy* **2011**, *36*, 15509.
[46] Y. Wang, L. Zhu, N. Ba, F. Gao, H. Xie, *Mater. Res. Bull.* **2017**, *86*, 268.
[47] Y. He, Z. Wu, L. Fu, C. Li, Y. Miao, L. Cao, H. Fan, B. Zou, *Chem. Mater.* **2003**, *15*, 4039.
[48] O. Lorret, D. Francova, G. Waldner, N. Stelzer, *Appl. Catal. B* **2009**, *91*, 39.
[49] H. Choi, D. Shin, B. C. Yeo, T. Song, S. S. Han, N. Park, S. Kim, *ACS Catal.* **2016**, *6*, 2745.

[50] S. S. Thind, G. Wu, A. Chen, *Appl. Catal. B* **2012**, *111–112*, 38.
[51] S. R. Gul, M. Khan, Z. Yi, B. Wu, *Materials* **2018**, *11*, 313.
[52] A. Siddiqa, D. Masih, D. Anjum, M. Siddiq, *J. Environ. Sci.* **2015**, *37*, 100.
[53] J. J. Brancho, B. M. Bartlett, *Chem. Mater.* **2015**, *27*, 7207.
[54] A. Kubacka, G. Colón, M. Fernández-García, *Appl. Catal. B* **2010**, *95*, 238.
[55] Y. F. Shen, T. Y. Xiong, T. F. Li, K. Yang, *Appl. Catal. B* **2008**, *83*, 177.
[56] J. X. Li, J. H. Xu, W.-L. Dai, H. Li, K. Fan, *Appl. Catal. B* **2008**, *83*, 233.
[57] M. Zhang, J. Wu, D. D. Lu, J. Yang, *Int. J. Photoenergy* **2013**, *2013*, ID 471674.
[58] A. Corma, S. Iborra, A. Velty, *Chem. Rev.* **2007**, *107*, 2411.
[59] J. C. Colmenares, R. Luque, *Chem. Soc. Rev.* **2014**, *43*, 765.
[60] M. Bellardita, M. Addamo, A. Di Paola, L. Palmisano, *Chem. Phys.* **2007**, *339*, 94.
[61] K. S. W. Sing, D. H. Everett, R. A. W. Haul, L. Moscou, R. A. Pierotti, J. Rouquerol, T. Siemieniewska, *Pure Appl. Chem.* **1985**, *57*, 603. 1685
[62] B. Sun, G. Zhou, Y. Zhang, R. Liu, T. Li, *Chem. Eng. J.* **2015**, *264*, 125.
[63] E. M. Samsudin, S. B. A. Hamid, *Appl. Surf. Sci.* **2017**, *391*, 326.
[64] T. Tachikawa, Y. Takai, S. Tojo, M. Fujitsuka, H. Irie, K. Hashimoto, T. Majima, *J. Phys. Chem. B* **2006**, *110*, 13158.
[65] F. Riboni, L. G. Bettini, D. W. Bahnemannd, E. Selli, *Catal. Today* **2013**, *209*, 28.
[66] W.-J. Yin, H. Tang, S.-H. Wei, M. M. Al-Jassim, J. Turner, Y. Yan, *Phys. Rev. B* **2010**, *82*, 045106.
[67] G. Kim, S.-H. Lee, W. Choi, *Appl. Catal. B* **2015**, *162*, 463.
[68] K. E. Sanwald, T. F. Berto, W. Eisenreich, O. Y. Gutiérrez, J. A. Lercher, *J. Catal.* **2016**, *344*, 806.
[69] I. A. Shkrob, T. W. Marin, S. D. Chemerisov, M. D. Sevilla, *J. Phys. Chem. C* **2011**, *115*, 4642.
[70] M.-H. Du, J. Feng, S. B. Zhang, *Phys. Rev. Lett.* **2007**, *98*, 066102.
[71] A. Di Paola, M. Bellardita, R. Ceccato, L. Palmisano, F. Parrino, *J. Phys. Chem. C* **2009**, *113*, 15166.
[72] Y. Xu, M. A. A. Schoonen, *Am. Mineral.* **2000**, *85*, 543.
[73] F. Tavakoli, A. Badiei, G. Mohammadi Ziarani, S. Tarighi, *Int. J. Environ. Res.* **2017**, *11*, 217.
[74] D. I. Kondarides, A. Patsoura, X. E. Verykios, *J. Adv. Oxid. Technol.* **2010**, *13*, 116.
[75] J. Yu, L. Qi, M. Jaroniec, *J. Phys. Chem. C* **2010**, *114*, 13118.
[76] R. Su, R. Tiruvalam, A. J. Logsdail, Q. He, C. A. Downing, M. T. Jensen, N. Dimitratos, L. Kesavan, P. P. Wells, R. Bechstein, H. H. Jensen, S. Wendt, C. R. A. Catlow, C. J. Kiely, G. J. Hutchings, F. Besenbacher, *ACS Nano* **2014**, *8*, 3490.
[77] M. Wu, M. Zhang, T. Lv, M. Guo, J. Li, C. A. Okonkwo, Q. Liu, L. Jia, *Appl. Catal. A* **2017**, *547*, 96.
[78] S. Cao, Y. Chen, H. Wang, J. Chen, X. Shi, H. Li, P. Cheng, X. Liu, M. Liu, L. Piao, *Joule* **2018**, *2*, 549.

Received: May 28, 2018

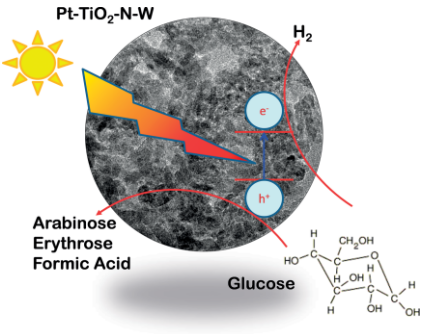

H_2 was produced with use of natural solar light irradiation by aqueous glucose reforming under green conditions with tungsten and nitrogen doped Pt-TiO_2 samples. Also, high value-added products were obtained from the partial oxidation of glucose. The highest H_2 production rate (ca. 1.0 mmol $gcat^{-1}$ h^{-1}) was observed in the presence of the Pt-TiO_2-W0.25 sample.

DOI: 10.1002/ejic.201800663